Parameter identification of 42CrMo4 steel hot forging plastic flow behaviour using industrial upsetting presses and finite element simulations

Gabriel Venet, Cyrille Baudouin, Corentin Pondaven, Régis Bigot, Tudor Balan

Parameter identification of 42CrMo4 steel hot forging plastic flow behaviour using industrial upsetting presses and finite element simulations

Gabriel Venet[1] · Cyrille Baudouin[1] · Corentin Pondaven[1,2] · Régis Bigot[1] · Tudor Balan[1]

Abstract
An experimental-numerical methodology was proposed for the parameter identification of constitutive laws, when applied to hot forging. Industrial presses were directly used to generate the reference experiments for identification. The strain and temperature heterogeneity that appears during on-press compression experiments was taken into account by an FE-based inverse method. Specific experiments were designed for the identification of the heat transfer and friction coefficients. A testing tool was designed and instrumented with displacement sensors and a force cell. This was then used on a hydraulic press and a screw press in order to cover a large range of strain rates. The identified parameter set was validated with respect to specialized plastometers, and a semi-industrial validation forging process. A reasonable accuracy was observed, particularly in realistic forging conditions.

Keywords Forging · Parameter identification · Industrial press · Constitutive law

Introduction

The correct description of the material behaviour during large deformation is necessary for the accurate numerical simulation of metal forming processes. The development of constitutive models is a fertile research field. Multiple physical mechanisms occur during the hot deformation of metals, including crystal slip, grain refinement, recovery, recrystallization, texture evolution, dislocation generation and pile-up, etc. Crystal-scale models were developed to explain many of these phenomena, while macroscopic-scale models were developed for industrial application. Following the early work of Avrami [1], macroscopic physically-based models were developed [2–4], along with more phenomenological laws which all ultimately describe the material's flow stress as a function of temperature, equivalent strain and equivalent strain rate phenomena [5–9]. Reviews of the most commonly used constitutive laws are available in [10, 11]. Several models proved their efficiency and are widely available in finite element (FE) simulation software.

Subsequently, the adaptation of such a model for a specific material requires the identification of a set of corresponding material parameters. The parameters are found with the help of inverse analysis, in order to best describe a set of experiments which reveal the material's behaviour. Advanced inverse methods have been developed specifically for large strain parameter identification during the hot deformation of metals [12–16]. Different optimization algorithms have been used in the literature for constitutive parameter identification. The most common ones in metal forming are either evolutionary algorithms, which are slower but better suited to find a global minimum, or gradient algorithms, which are faster but may converge to a local minimum. Both approaches were compared in the literature [17, 18] and proved to be efficient; they are commonly available in commercial software [19]. As a consequence, the most important step is the experimental characterization of the material over strain, temperature and strain-rate ranges relevant to the foreseen applications. In the literature, many tests are recommended for assessing the rheological properties of a material: tensile, torsion, shear or compression tests; their respective variants, advantages and limitations were exhaustively explored in the literature, e.g. [20]. Specific parameter identification methods were developed in

✉ Tudor Balan
tudor.balan@ensam.eu

[1] Arts et Metiers Institute of Technology, Université de Lorraine, LCFC, HESAM Université, F-57070 Metz, France

[2] ACM - ABS Centre Métallurgique, 10 rue Pierre Simon de Laplace, F-57070 Metz, France

order to determine both rheology and tribology parameters within the same experiment, in quasi-static or high strain-rate conditions [21, 22].

In the literature, the uniaxial compression test is very popular for metal forming applications due to its simplicity and ability to explore large ranges of strain and strain rate. For example, uniaxial compression was used in [23] to compare different constitutive models, in [24] to identify the parameters of an internal variable constitutive model, and in [25, 26], where an artificial neural network was used as a metamodel for the inverse analysis. In these works, the compression experiments are performed using specialized plastometers, specifically designed to apply large constant strain rates during the tests, along with rapid heating, constant temperatures, and minimal friction. As a consequence of these mature developments, models and material parameters were determined for the most common metal-forming materials, and complete material databases were produced and commercialized. As their accuracy, robustness and completeness increased over time, such databases are now the main source of material parameters in industrial application.

Nevertheless, recent developments in metal forming methods require new parameter identifications. On the one hand, new materials are developed in order to improve the strength-ductility balance and answer environmental constraints. On the other hand, customization, as well as ever tighter deadlines and cost constraints, increase the needs for process simulation. While the available models can often cover the response of new materials, their missing parameters are often determined using degraded procedures, mainly based on the tensile test results supplied with every material batch by material suppliers. This leads to the paradox that poor material data is often used in industry, in spite of the availability of powerful identification methodologies.

This paper explores the possibility of using industrial presses to characterize bulk materials for constitutive model parameter identification on industrial site, instead of quasi-homogeneous characterization experiments on specialized plastometers. The specific question addressed in this paper is: can industrial users perform parameter identification using only their industrial equipment and knowledge? An experimental and numerical methodology is proposed, which is further validated with respect to a more traditional identification procedure; a semi-industrial forging process is used for validation. The paper is organized as follows. Section 2 describes the equipment, materials, and experimental procedures used in the investigation, while the applied simulation methods and models are described in Section 3. The experimental results are reported in Section 4, and they subsequently serve in Section 5 for the parameter identification. The discussion in section 6 leads to the final Conclusion.

Experimental methods

Experimental procedures, materials and equipment

Uniaxial compression tests were performed at various temperatures and strain-rates. The compression experiments were realized using two industrial presses. In addition, two specialized testing machines were used for validation purposes. Each of these machines came with a specific heating device and required specific sample dimensions.

The tested material was 42CrMo4 steel, delivered as rolled bars of 30 mm diameter, in an annealed state. The chemical composition and tensile properties of the material are summarized in Table 1. Several bars were purchased at the same time from a unique batch. This standard steel is well documented in the scientific literature and several databases provide reliable material data, including parameters for various constitutive laws and deformation conditions.

Two presses were used for the core experimental campaign: a Loire 6MN hydraulic press and a Lasco 31.5 kJ screw press, both belonging to the Vulcain experimental platform at Arts et Metiers in Metz. These two machines provide very different forging speeds. The hydraulic press provides a nominal ram speed of 30 mm/s, which is constantly maintained during the test. The impact ram speed can be set to values up to 680 mm/s on the screw press. During the experiment, the kinetic energy of the ram is transformed in part deformation energy, thus the ram speed significantly decreases during the test. Consequently, the two machines allow for compression tests at different strain rates: in the range of 1 s^{-1} for the hydraulic press and 10 s^{-1} for the screw press, for the selected sample geometry.

For the compression experiments on industrial presses, 60 mm tall cylindrical billets were cut, with a 30 mm diameter (the original bar diameter). The actual dimensions (height / diameter) of each sample were measured in three equally distributed locations each, and the actual dimensions of each sample were further used when exploiting the experimental measurements or during the numerical simulations.

The lubricant used on the presses was Bonderite L-GP D31A, a spray lubricant that provides a graphite coating on the tools. Ring compression experiments were used for friction characterization. The geometry of the ring samples was as follows: height 20 mm, inner diameter 35 mm and outer diameter 70 mm. Consequently, an additional 42CrMo4 bar was purchased in a larger diameter in order to prepare the friction test samples.

The samples were heated using an electrical oven next to the presses, under a controlled atmosphere to avoid oxidation. The oven provides nominal temperatures of up to 1250 °C. For each test series, the oven was heated up to the required temperature and then the samples were introduced into the oven and left for a period of 20 min, in order to obtain a

Table 1 Composition and tensile properties of the raw 42CrMo4 material used in the experiments

Element	C	Cr	Mn	Si	Cu	Ni	Mo	S
Mass %	0.40	0.95	0.76	0.14	0.21	0.08	0.17	0.015
Yield stress [MPa]		Ultimate tensile strength [MPa]				A5 max. Elongation [%]		
797		1046				12.7		

uniform temperature within the billets. After this heating step, the samples were extracted from the oven one by one and tested. Consequently, the waiting time in the oven varied for each sample between 20 and 35 min.

Additional compression experiments were performed for validation purposes using two specialized plastometers. The first plastometer was a Gleeble 3800 simulator, often used in the literature for thermomechanical material characterization of various steel grades [27] and other alloys, either through tensile testing [28] or compression testing [26]. In the current work, uniaxial compression tests were carried out on cylinders 12 mm high and 10 mm in diameter. Specific 0.25 mm thick layers of graphite foils were used to reduce friction. The test temperature was reached by resistance heating and was controlled through the testing process with a thermocouple fixed on the billet. All experiments were performed by the Instytut Metelurgii Zelaza in Gliwice, Poland [29]. The second specialized testing device was a DIL805 A/D plasto-dilatometer. Friction was reduced with molybdenum foils. An induction coil placed around the sample performed the heating and a thermocouple welded on the surface of the billet controlled the heating. Experiments were carried out at ACM - ABS Centre Métallurgique in Metz, France. On the Gleeble and DIL805 machines, the heating time was 5 to 7 mins depending on the desired temperature, followed by a 30 s waiting time for temperature homogenisation. A constant temperature was maintained during the tests on these two machines with the aid of a thermocouple welded onto the outer surface of the billet, in its central cross-section. The tool displacement was controlled, in order to maintain a constant average strain-rate during each compression test.

Displacement and force measurement on press

The Gleeble and DIL805 machines are equipped with displacement sensors and load cells installed close to the compression sample, while the sensors of the industrial presses are relatively far from the samples. Consequently, the measured quantities may include not only the response of the sample, but also the response of the tooling and the machine. Preliminary tests demonstrated that the force measurements on the screw press were significantly affected by the vibratory response of the press. The displacement measurements were more accurate, but could be affected by the stiffness of the tooling pile-up and thus could induce dispersion from one experiment series to another (for example, after a change of tooling). Consequently, a simple, specific tool was designed and manufactured for this study, shown schematically in Fig. 1. The displacement between the upper and lower dies was measured with three Micro-Epsilon optoNCDT 1401 laser sensors. The position of the displacement sensors ensures that only the displacement between the dies is measured, without any perturbation from the press due to the elastic deformation [30] or the backlash between the different parts of the press / tool. The load is recorded by a SCAIME ML11 load cell on which the lower tool is screwed, thus measuring the force passing through the sample as close as possible to it. The upper die is a regular flat die. For very high strain rate experiments it may sometimes be necessary to consider the elastic response of the testing tools in order to correctly extract the material response from the actual experimental data [31]. However, in our case, the dynamic effects appeared to be insignificant, even on the screw press, and the load-displacement curves showed no spurious oscillations when measured at the bottom of the lower die.

Temperature monitoring experiments

The material temperature is neither constant nor uniform during the compression experiments on the presses. The press environment also makes temperature measurement inadequate during the experiments. As a consequence, the temperature evolution during the transfer from the oven to the press, and

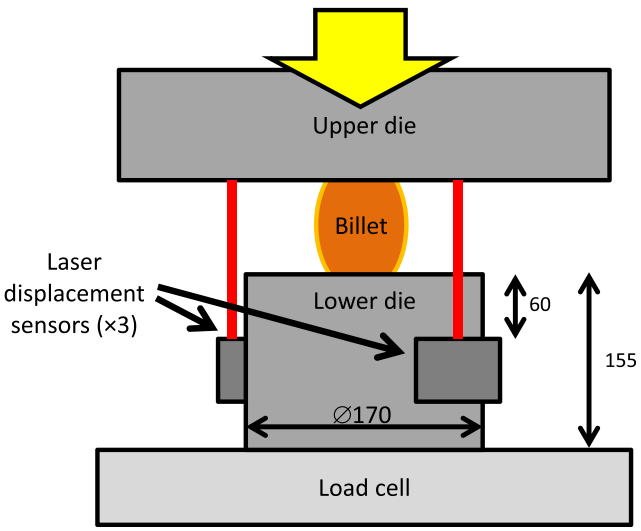

Fig. 1 Outline of the compression test tooling on industrial presses, including displacement sensors and force cell. Dimensions in mm

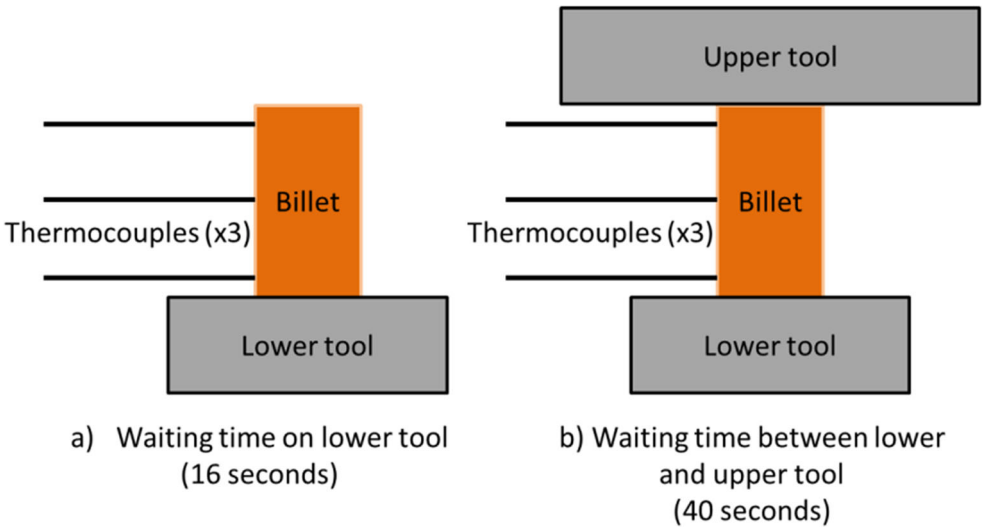

Fig. 2 Outline of the last two steps of the thermal experiment. The billet rests on the lower tool (a) and is then maintained under pressure between the lower and upper tools (b)

throughout the tests, must be included in the simulations. The predicted temperature evolution and distribution depend on the thermal properties of the material, and the thermal interface with the tools and the air. Therefore, four parameters must be identified: the emissivity of the material, the exchange coefficient with air, the exchange coefficient with the dies without pressure and the exchange coefficient with the dies during compression. Experimental measurements were designed and performed specifically to identify these parameters. The experiments used the same compression billets, equipped with three thermocouples welded onto the lateral surface: one at 10 mm distance (±3 mm) from the upper surface of the billet, one at mid-height and one at 10 mm from its lower surface. The billet was heated in the oven at 1000 °C and then manually transferred to the press in 6 s. After a 16 s waiting time, the press was set to apply a small pressure on the billet, without deforming it plastically. The temperatures were measured during an additional 40 s period, under pressure. The two last steps of the process are schematically shown in Fig. 2.

Simulation models

Two simulations approaches were used in the present investigation. The simulation of the quasi-homogeneous compression tests on plastometer was carried out using the slab method [32], in order to account for the friction effect, while the temperature and strain rate were considered constant and uniform within the sample. This approach has been shown to be sufficiently accurate for the analysis of plastometer characterization experiments and it is regularly used [14, 27]. However, for the simulation of the on-press experiments, full-field FE simulations were performed using the commercial Forge® software.

FE simulation model for the compression tests on press

The Forge® software handles large strain thermo-plasticity, contact and friction. Two-dimensional simulations were performed using the built-in linear triangular finite elements. A preliminary convergence study led to a

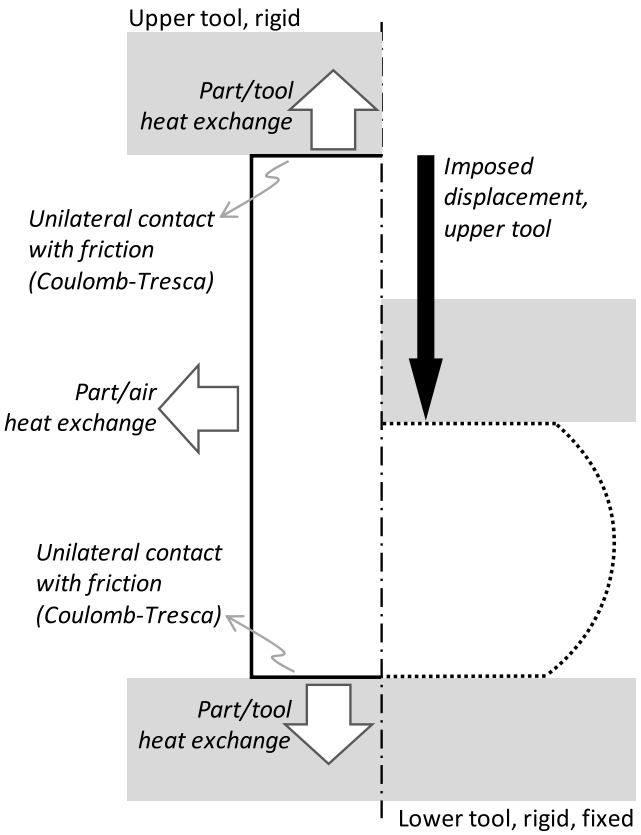

Fig. 3 Boundary conditions used for the simulation of the compression tests on press

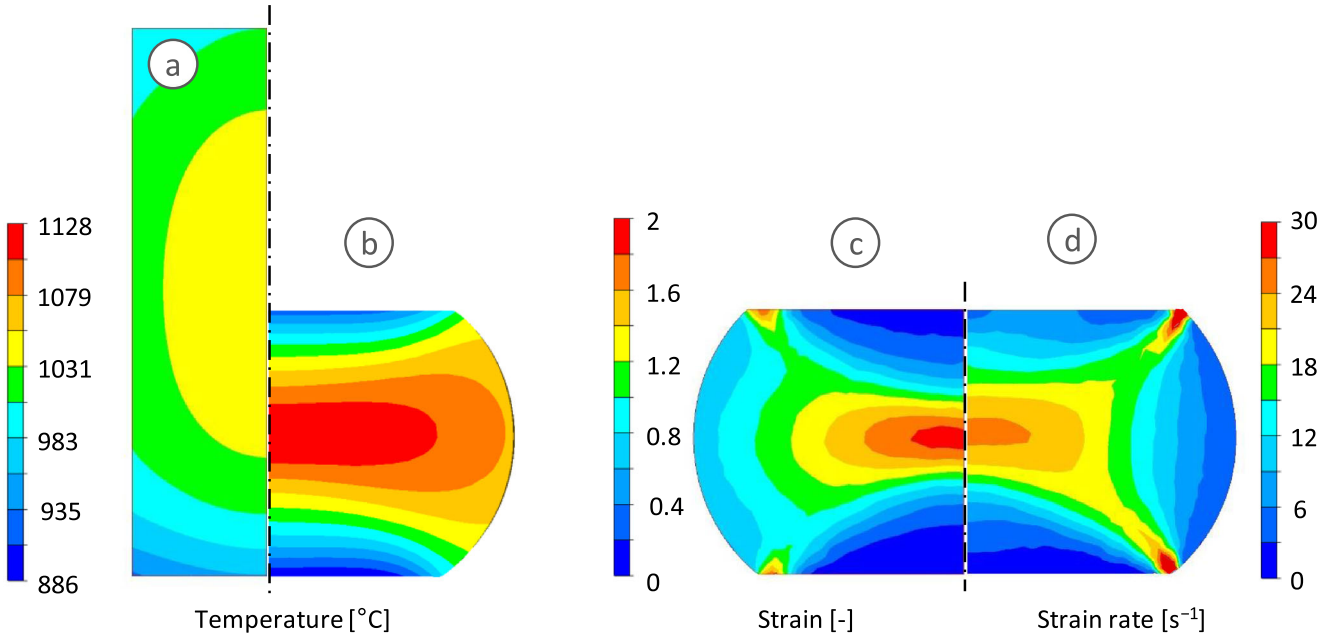

Fig. 4 Gradients of a) initial and b) final temperature, c) strain and d) strain rate after the simulation of a uniaxial compression test on the screw press, with 1100 °C initial (oven) temperature

uniform mesh size of 1.47 mm. Simulations with and without remeshing led to the same results, in terms of forging load, within an error limit of ±3%. Therefore, the same mesh was used throughout the simulations. The boundary conditions used in the simulations are summarized in Fig. 3. The upper and lower tools were modelled as rigid bodies and unilateral contact with friction was prescribed at the part/tool interfaces. Heat transfer was allowed between the part and the tools, and between the part and the air, respectively. The lower die was fixed, while a prescribed vertical displacement was imposed to the upper tool. In the case of the hydraulic press, a constant tool velocity was imposed, equal to the constant velocity of the press ram in the experiment. For the screw press, the experimental stroke-time history for each experiment was imposed on the corresponding simulation. A total 35 mm compression stroke was imposed on all of the simulations. In the experiments, the final stroke was larger than 35 mm in all cases and the experimental curves were trimmed to this value in view of the parameter identification. In order to take into consideration the heterogeneous temperature distribution at the beginning of the compression experiments, the simulation included three steps. In the first step, the temperature evolution was determined during the transfer of the billet between the oven and the press.

Table 2 Hensel-Spittel parameter values for 42CrMo4 steel in the Forge® software material database

A [MPa]	m_1	m_2	m_3	m_4	m_5	m_7	m_8	m_9	ε_0
1872	−0.0029	−0.11	0.144	−0.049	0	0	0	0	0

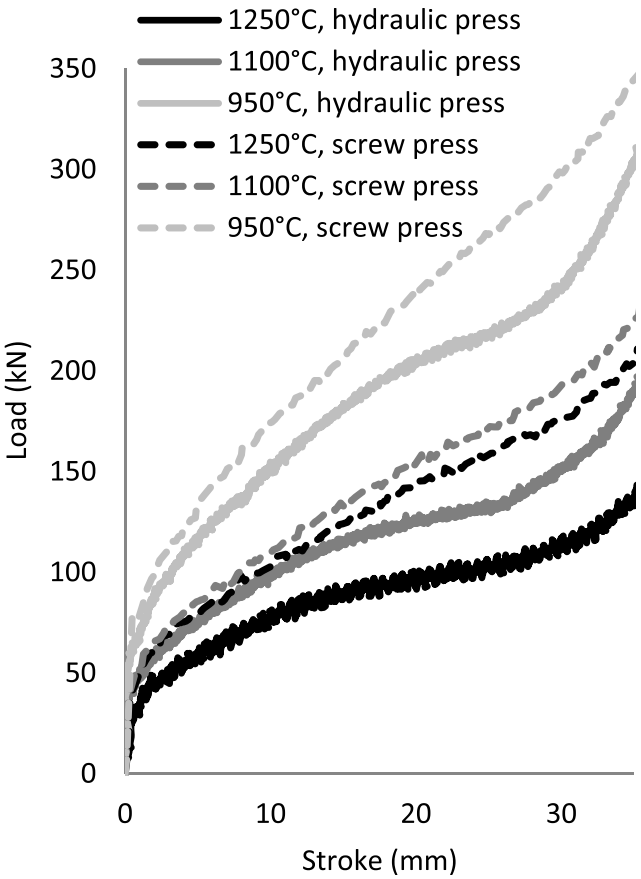

Fig. 5 Experimental force/displacement curves of the compression tests on industrial presses

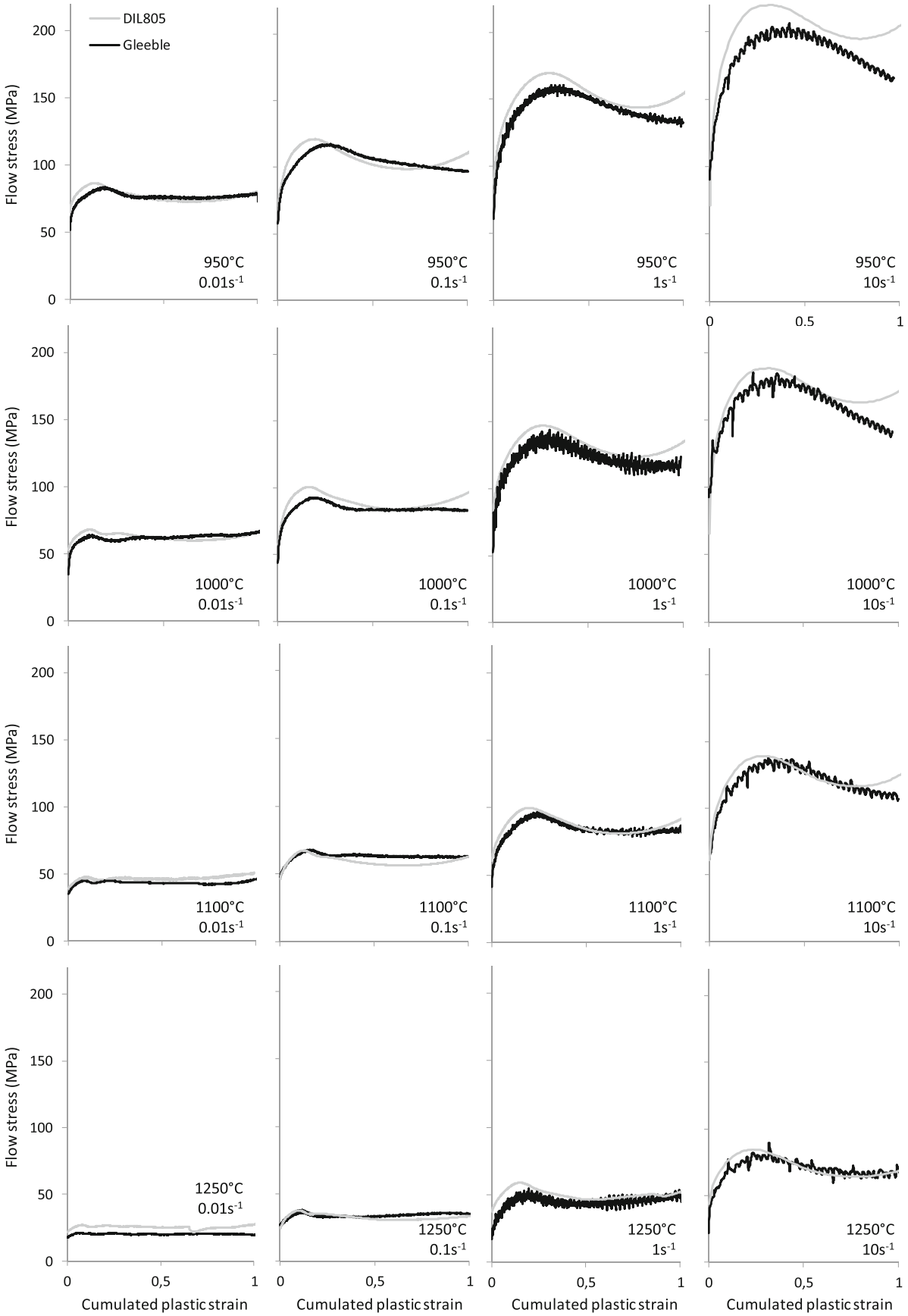

Fig. 6 Comparison of flow stress versus cumulated plastic strain curves for the Gleeble (black) and the DIL805 (grey) plastometers

Heat exchange with air was imposed on the entire boundary of the billet. In the second step, the temperature evolution was simulated for the time when the billet was on the lower tool, but the deformation had not yet start. Finally, the third step simulated the actual compression test, using the boundary conditions described in Fig. 3. The transfer times for the first two steps were those measured experimentally for each test.

Due to the temperature and friction boundary conditions during the test, heterogeneous distributions of temperature, strain and strain rate were obtained in the billet during deformation. Figure 4 illustrates the corresponding gradients within a sample after a typical compression test on the screw press. These gradients justify the use of an FE-based analysis of the compression tests during the parameter identification phase. It is, however, important to note that these temperature, strain and strain rate distributions had the same pattern for all samples and testing conditions. The heat transfer, friction and rheological parameters used in this simulation are those from Tables 3-5, respectively.

Hensel-Spittel rheological equation

Several visco-plastic constitutive laws are available in Forge®, along with a significant database of material parameters, including for 42CrMo4 steel at cold and hot forging temperatures. The Hensel–Spittel equation [7] was selected for this work:

$$\sigma = A e^{m_1 T} (\varepsilon + \varepsilon_0)^{m_2} \dot{\varepsilon}^{m_3} e^{\frac{m_4}{(\varepsilon+\varepsilon_0)}} [1 + (\varepsilon + \varepsilon_0)]^{m_5 T} e^{m_7(\varepsilon+\varepsilon_0)} \dot{\varepsilon}^{m_8 T} T^{m_9}, \quad (1)$$

where σ designates the flow stress, ε the equivalent strain, $\dot{\varepsilon}$ the equivalent strain rate, and T the temperature, while A, ε_0 and m_1 to m_9 are rheological parameters. The parameter set proposed in the Forge® material database for material 42CrMo4 is summarized in Table 2. This equation reduces to several classical models by setting some of the parameters to zero. With all of the parameters active, this equation does not represent specific physical deformation mechanisms but it has an increased mathematical flexibility. One drawback is that its predictions may significantly deviate from reality outside of the experimental identification range [33]. Here, the model was only used in the of strain, strain-rate and temperature ranges covered by the experiments.

Experimental characterization results

For the identification of the parameters in Eq. (1), six different test conditions were explored on the industrial presses: three initial temperatures on each machine. In addition, characterization experiments were also conducted on two plastometers. The resulting experimental curves are summarized in this section.

Press-based compression experiment results

Three oven temperatures were chosen, typical for steel hot forging conditions: 950 °C, 1100 °C and 1250 °C. Each temperature was tested on the hydraulic press and on the screw press. Each test was repeated three times to verify repeatability, which was found to be very good on both presses. Figure 5 summarizes the selected curves to be further used for the parameter identification process. The series exhibits significant

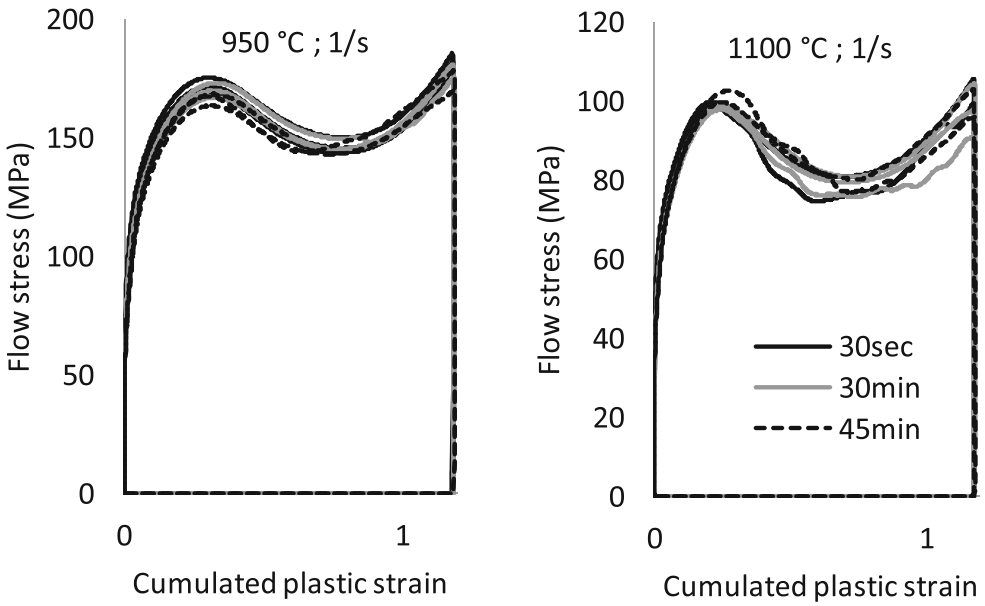

Fig. 7 Influence of temperature holding time on two stress/strain curves of 42CrMo4 steel

Table 3 Heat exchange parameter values after identification

Exchange coefficient with air (Wm^{-2} K^{-1})	Emissivity coefficient	Exchange coefficient with lower tool (Wm^{-2} K^{-1})	Exchange coefficient with tools under pressure (Wm^{-2} K^{-1})
10	0.95	680	1715

effects of both temperature and strain-rate, thus offering theoretical premises for discriminant parameter identification.

Characterization results on specialized plastometers for validation

Figure 6 displays the stress/strain curves obtained for various temperature and strain rate values with the Gleeble and DIL805 plastometers. Considering that the temperature and strain rate were constant and homogeneous within the sample during the test, it was possible to analytically convert the measured force/displacement curves into stress/strain curves with the slab method. The maximum difference between the Gleeble and DIL805 curve pairs varied between 11% (at 1250 °C/0.01 s^{-1}) and 23% (at 950 °C/10 s^{-1}). Most of the time, the DIL805 plasto-dilatometer gave slightly higher stress values. In particular, the first peak stress was larger with the DIL805 plasto-dilatometer; the differences ranging between 0.2% and 18%, with an average gap of 6.7%. For the case of 1250 °C and 0.01 s^{-1}, a difference of 31% was observed, however, this only corresponds to an absolute difference of 6 MPa. The stress evolution at large strains (beyond 0.7) was slightly different, with the Gleeble results exhibiting stress stagnation or softening while the DIL805 plasto-dilatometer results showed apparent resumption of hardening. These differences would only have a minor impact on the results of the comparisons performed in this paper. Therefore, for the rest of this paper, we will only consider the results given by the Gleeble equipment, as a reference for the specialized devices. Nevertheless, the material behaviour described by the two experimental series was sometimes different, for example the change in the sign of the hardening slope for some of the experiments, at large strains. In the context of the present investigation, it is important to bear in mind that plastometer experiments are not entirely exempt of artefacts induced by temperature variations, friction and other testing parameters. The characterization of metals at high temperature and strain still remains a significant challenge.

Since the heating time was very different between the presses and plastometers, additional compression tests at 1100 °C and 950 °C at a strain rate of 1 s^{-1} were carried out after different temperature holding times, using the DIL805 plasto-dilatometer. As shown in Fig. 7, there was no significant influence of holding time on the stress-strain material response (although it is probable that there were differences at a microstructural scale). As a consequence, one can safely assume that using an oven for heating the billet did not significantly influence the compression test results.

Parameter identification results

The identification of the material parameters was mainly performed using the built-in optimization algorithm in Forge®. This is based on a genetic algorithm using a kriging

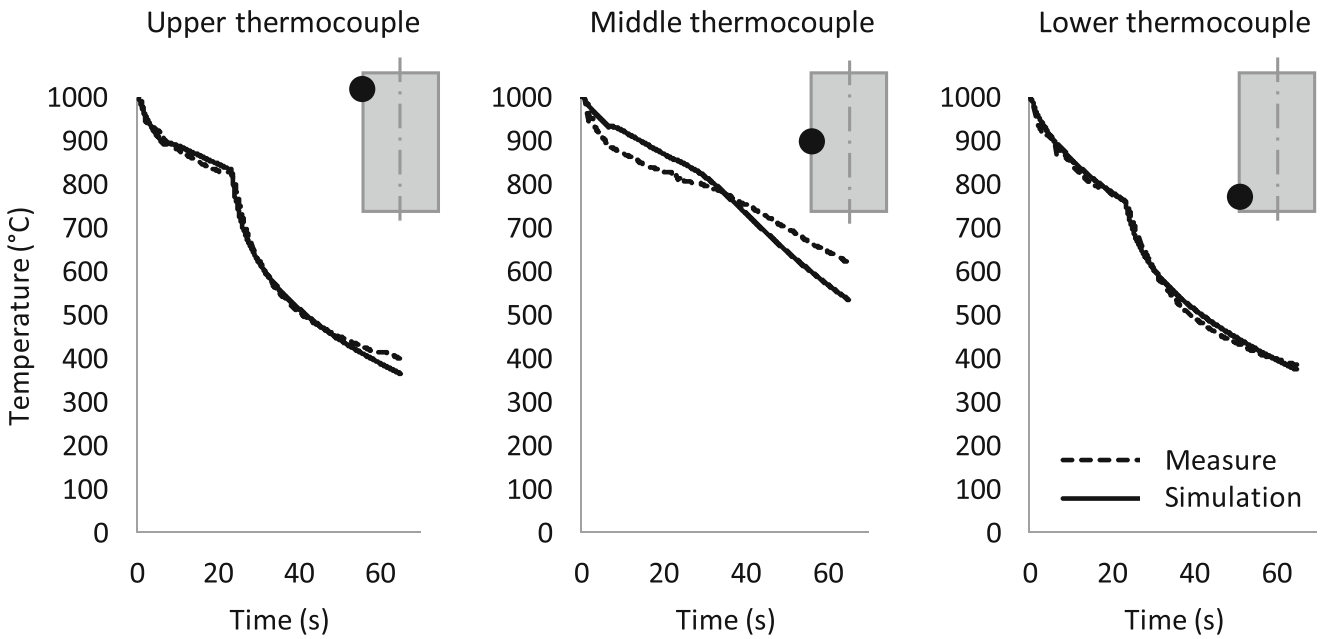

Fig. 8 Comparison between measured and simulated temperature evolution at the three locations on the billet's surface during the cooling experiment

Table 4 Friction coefficients found by the ring test with 70 mm outer diameter, 35 mm inner diameter 35 mm and 20 mm height

Friction coefficient	Hydraulic press	Screw press
$\overline{m}$ (Tresca)	0.4	0.2
μ (Coulomb)	0.231	0.115

metamodel [34]. The cost function, that is minimized by the algorithm, can be written as

$$CF = \frac{1}{N}\sum_{i=1}^{N}\sqrt{\frac{\sum_{j=1}^{n_i}\left(a_{i,j}^{exp}-a_{i,j}^{calc}\right)^2}{\sum_{j=1}^{n_i}\left(a_{i,j}^{exp}\right)^2}} \quad (2)$$

where $a_{i,j}^{exp}$ is an experimental quantity measured at the step j of test i, and $a_{i,j}^{calc}$ is the same quantity obtained by calculation. N is the number of tests, while n_i is the number of steps in the considered test. When plastometers are used, the flow stress can be calculated with the Hensel–Spittel eq. (1) and this is directly used (quantity a) in the cost function expression (2). In the case of the heterogeneous experiments realized on the press, the cost function uses forces, both experimental and simulated by finite elements. The inverse analysis is performed with the help of an evolutionary algorithm and a generalized reduced gradient algorithm. The two algorithms were used iteratively: first, the evolutionary algorithm was used to span the entire solution range, followed by the gradient algorithm to optimize the result. This procedure was repeated for several initial guesses in order to prevent premature convergence on local minima.

In order to allow for the accurate FE simulation of the compression tests on the press, the heat transfer and friction parameters had to be identified first.

Heat transfer and friction parameters

The heat transfer parameter identification is based on the specific experiments described in Fig. 2. These experiments were simulated using Forge® and the built-in optimization algorithm of Forge® was used to minimize the difference between the measured and the simulated temperature/time curves until the optimal parameters were found.

The identified parameters are reported in Table 3 and the result of the FE simulations with these parameters is displayed in Fig. 8. The temperatures of the lower and upper thermocouple are very well described by the simulation. Concerning the thermocouple in the middle of the billet, differences up to 10% (50 °C) were observed between the simulation and the measurements. The thermal parameters in Table 3 were used in the rest of this paper. The specific heat (460 J/kg·K) and thermal conductivity (46 W/m·K) were taken from the literature.

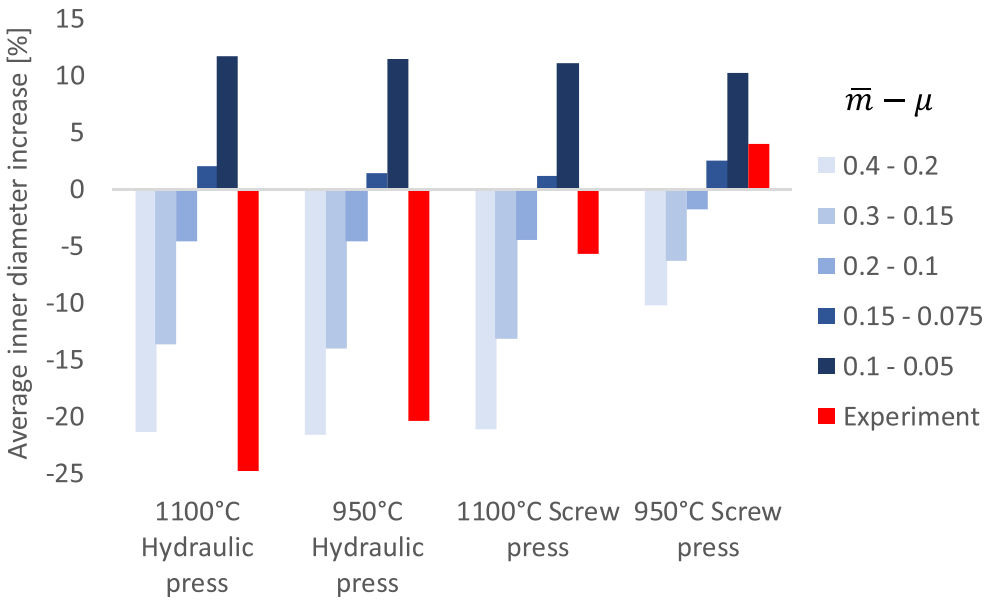

Fig. 9 Influence of friction coefficients on the samples' inner diameter variation after the ring compressions tests

Table 5 Hensel-Spittel parameter values after identification on industrial presses, using unconstrained identification (case 1) and physically-based bounds (case 2). Parameter A is in MPa; all other parameters are dimensionless

case	A	m_1	m_2	m_3	m_4	m_5	m_7	m_8	m_9	ε_0
1	260	−0.0036	−1.08	0.063	−0.28	-8×10^{-5}	0.87	6.8×10^{-5}	0.34	0.13
2	1714	−0.0036	0.129	0.0026	2×10^{-6}	3×10^{-5}	−0.26	0.00016	0.16	0.01

Finally, the friction model used in the simulation is a combined Coulomb–Tresca model, typical for bulk forming simulation. It has two parameters, one related to Coulomb's law (denoted μ) and the other related to Tresca (denoted $\overline{m}$). These parameters were identified with a FEM inverse analysis using the ring test and a cost-function based on the final inner diameter of the ring (see e.g. [35] for the detailed methodology). The initial stages of the ring test do not allow for an accurate

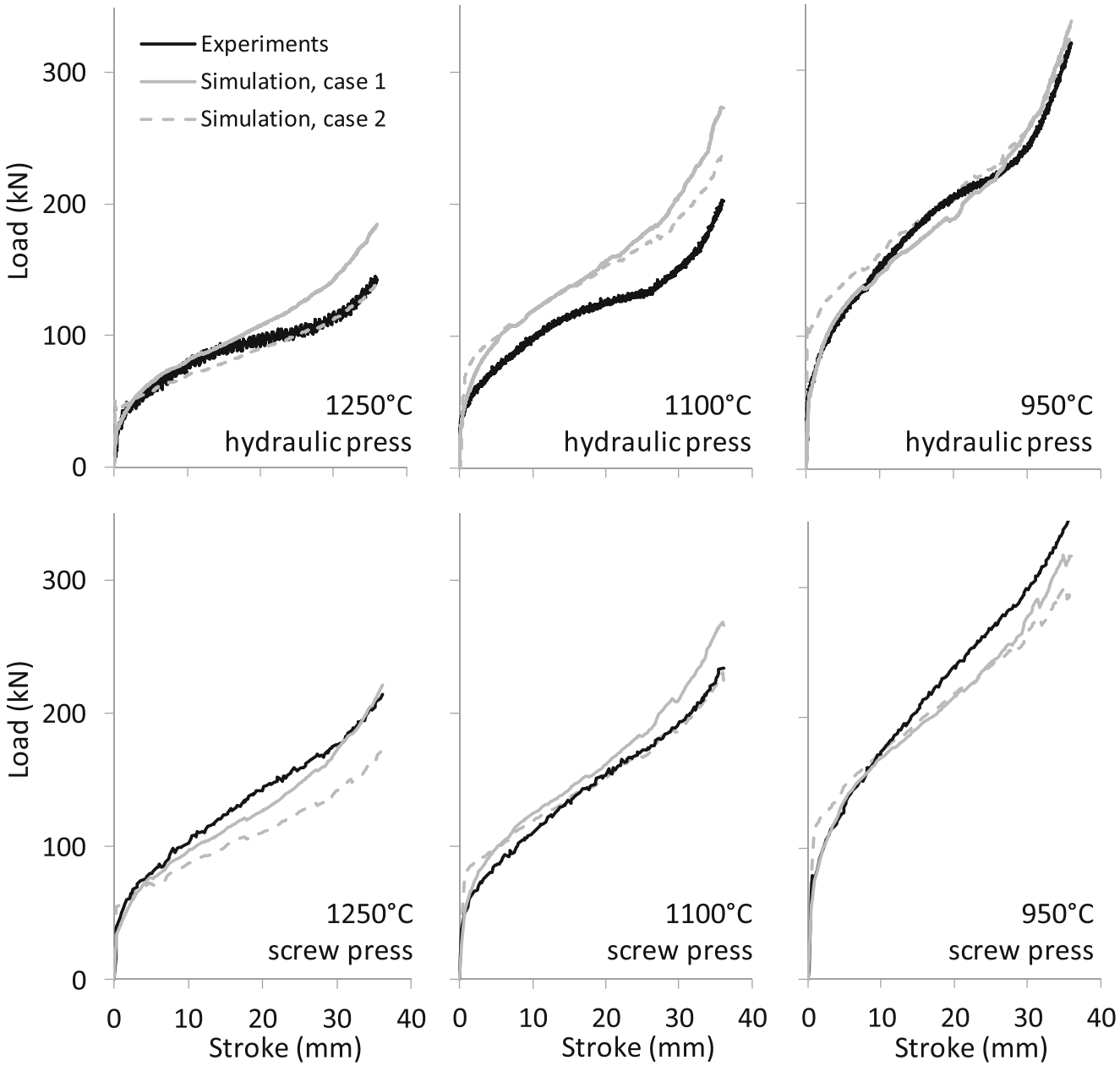

Fig. 10 Comparison between the force-displacement curves measured experimentally and those predicted by FEM with the identified parameters

Table 6 Hensel-Spittel parameter values after identification using the Gleeble experimental data

case	A	m_1	m_2	m_3	m_4	m_5	m_7	m_8	m_9	ε_0
1	1810	−0.0035	−0.82	0.039	−0.29	19×10^{-5}	0.29	9×10^{-5}	0.098	0.18
2	1756	−0.0036	0.13	0.003	6×10^{-6}	-8×10^{-5}	−0.31	0.00013	0.17	0

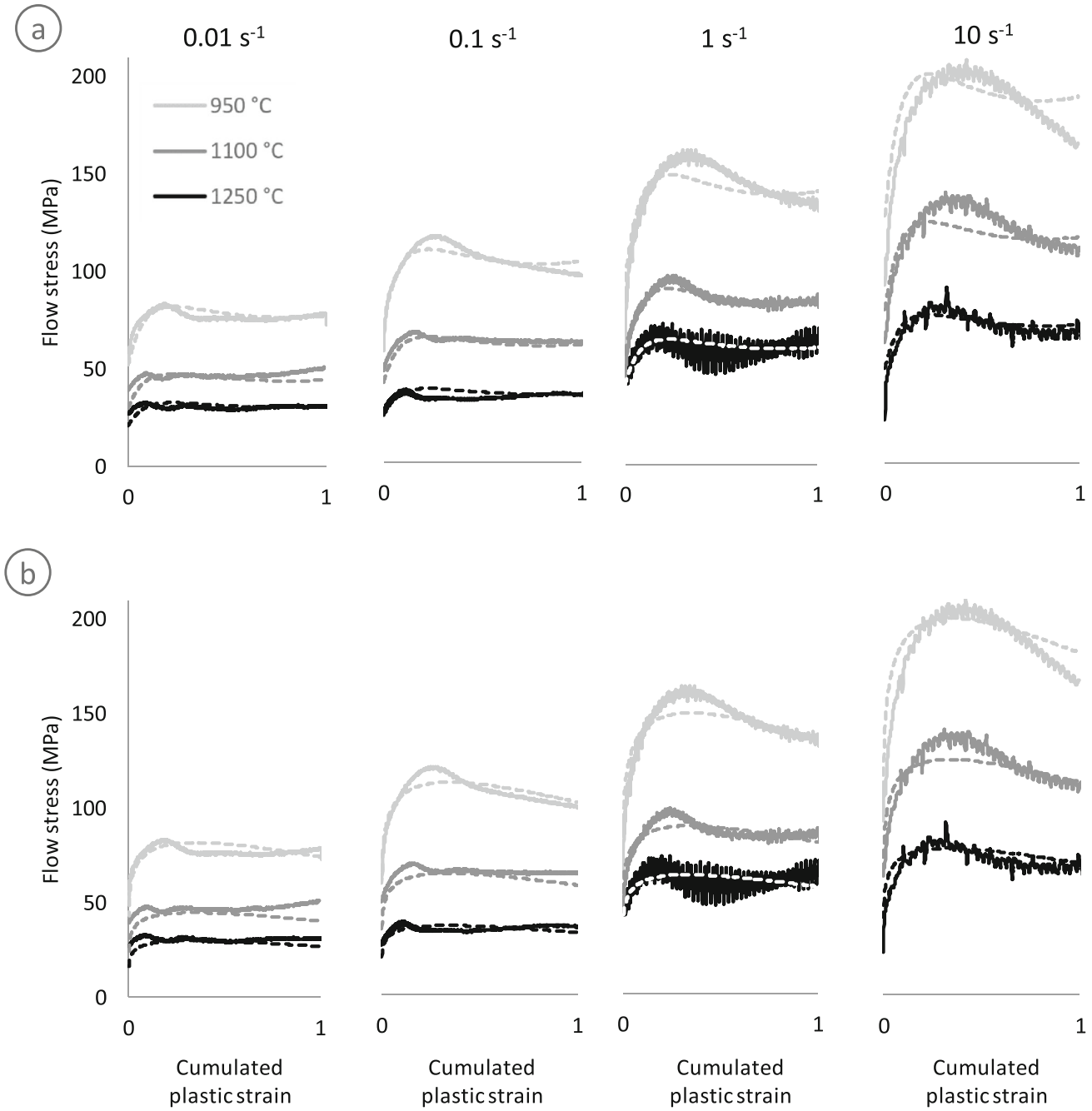

Fig. 11 Flow stress versus cumulated plastic strain curves obtained using the Gleeble experimental data: experimental (solid lines) and calculated with the identified parameters (dashed lines) a) under unconstrained optimization and b) under consideration of the physically-based constraints $m_2 > 0$, $m_4 > 0$ and $m_7 < 0$

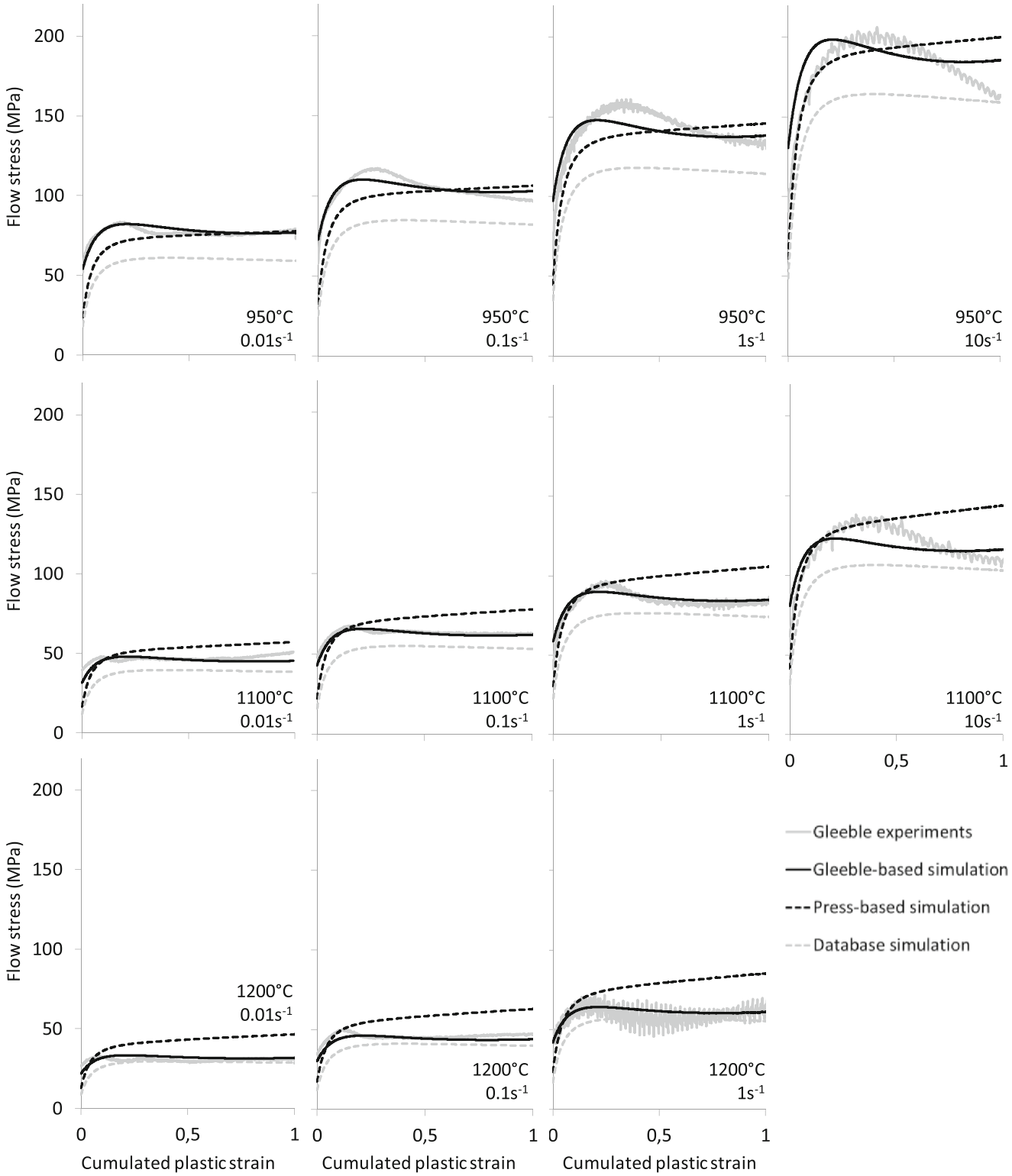

Fig. 12 Stress/strain curves based on the parameters identified (unconstrained minimization) with the Gleeble and the industrial presses, the Gleeble experimental data and simulated curves with the Forge® database parameters

determination of Coulomb's coefficient of friction but it was assumed that $\frac{m}{\mu} = \sqrt{3}$. Ring compression experiments were performed at 950 °C and 1100 °C on the two presses. Each experiment was repeated three times; the variability of the inner diameters was within ±2 mm maximum. The experimentally measured variations of the inner diameter for these

Fig. 13 Semi-industrial validation part: dimensions (left), experiment (center), simulation (right)

four configurations are plotted in Fig. 9, along with the simulated results for various sets of friction coefficients numerically tested for identification. It is noteworthy that the friction coefficients may be sensitive to the sliding speed [36–38]. Consequently, two sets of friction parameters were identified: one for the hydraulic press and one for the screw press. These two parameter sets are given in Table 4.

All of these parameters were used for all of the subsequent simulations in the paper.

Hensel-Spittel equation parameter identification using the press-based experiments

The ten parameters in Eq. (1) were identified with respect to the press-based experimental force-displacement curves in Fig. 5. Two identification strategies were compared. In the first case, an unconstrained minimization of the cost function was performed. In the second case, a set of physically-based constraints were used to bound the values of some parameters: condition $m_2 > 0$ was enforced for the hardening term, while conditions $m_4 > 0$ and $m_7 < 0$ were imposed for the softening terms. The identified parameters are shown in Table 5 and Fig. 10 shows the experimental force/displacement curves, as well as the curves obtained by FE simulation with the identified parameters. The experimental trends of the temperature and strain-rate influence are correctly reproduced in the simulations, using both parameter sets. For four curves out of six, the simulation-experiment differences are in the range of the experimental scatter. The largest gap (30%) between simulation and experiment data for the unconstrained identification case was observed for a 1100 °C oven temperature on the hydraulic press. The average difference between simulated and experimental loads was 8% for the unconstrained identification and 10% for the physically-bound identification, over the entire set of experimental values used for the identification. According to Fig. 10, both parameter sets describe with similar accuracy the experiments. In these conditions, it is generally accepted that the usage of physical bounds leads to more robust solutions, in particular when applied outside of the experimental range of conditions. This is specifically true for large strains and large strain rates, since both are limited in experiments.

In order to explore in more detail the validity of these results, a classical parameter identification was also performed

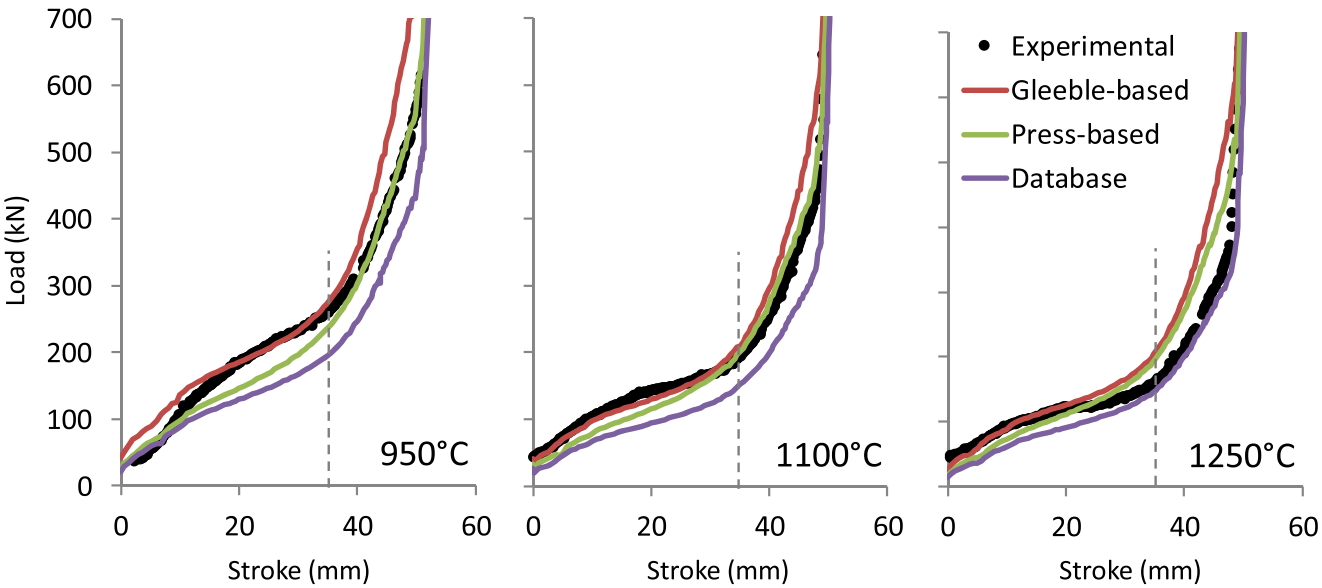

Fig. 14 Force/displacement curves: experimental (symbols) and simulated (lines) with the three parameter sets. The vertical dashed line indicates the 35 mm split line further used to analyse the results in Fig. 16

using the plastometer-based characterization, presented below.

Hensel-Spittel equation parameter identification using plastometer experiments, for validation

The results of the parameter identification with respect to the Gleeble plastometer experiments are shown in Fig. 11 and the corresponding Hensel-Spittel parameters are summarized in Table 6. In both cases (constrained / unconstrained minimization), the predictions were close to the reference curves and followed the correct trends. However, the shape of the curves was clearly not the same. The results showed a better compliance between predictions and experiments for unconstrained minimization at the larger temperatures (softening followed by stagnation), while, at lower temperature values, the compliance was better for the constrained minimization. In particular, the first peak stress was both too wide at a low strain rate but too small at a high strain rate, compared to the reference values. This is not surprising considering that the shape of the curve has little weight in the cost function compared to the average stress values. The predicted hardening slopes at the end of each curve are also significantly different. It is clear that the large strain predictions of the two parameter sets will be more and more different, with the unconstrained identification leading to potentially unrealistic predictions at large strains. On the other hand, the differences between predictions and experiments are in the same range as the differences between the two series of reference experiments in Fig. 6, thus reaching a significant limit towards possible improvement. It is noteworthy that the differences between the two sets of predictions are also comparable (both quantitatively and qualitatively) to the differences observed between the two sets of experimental curves in Fig. 6. For the subsequent comparisons, the results of the unconstrained minimization were used, which led to a cost function that was approximately 10% smaller than for constrained minimization.

Discussion

The parameter sets obtained with the proposed parameter identification methodology (Table 5) were not identical to the ones obtained by the classical approach (Table 6). Since the two procedures used different experimental data as reference for the identification, the comparison task is not straightforward. For example, the two parameter sets can be used to predict stress-strain responses at a constant temperature and strain-rate. These predictions can be further compared to the Gleeble-generated experiments, as shown in Fig. 12.

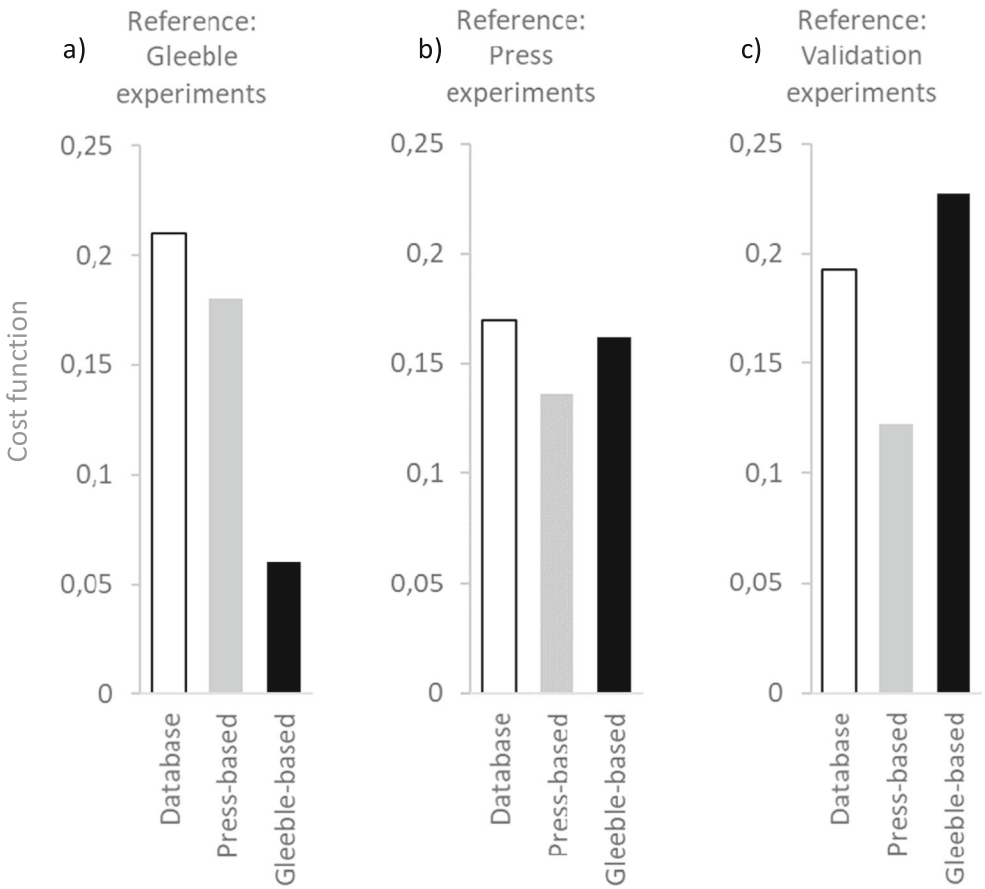

Fig. 15 Difference in cost function between the predictions of the three sets of parameters (database, press-based and Gleeble-based) with respect to various reference data: a) Gleeble compression experiments, b) press compression experiments and c) semi-industrial part forging experiments

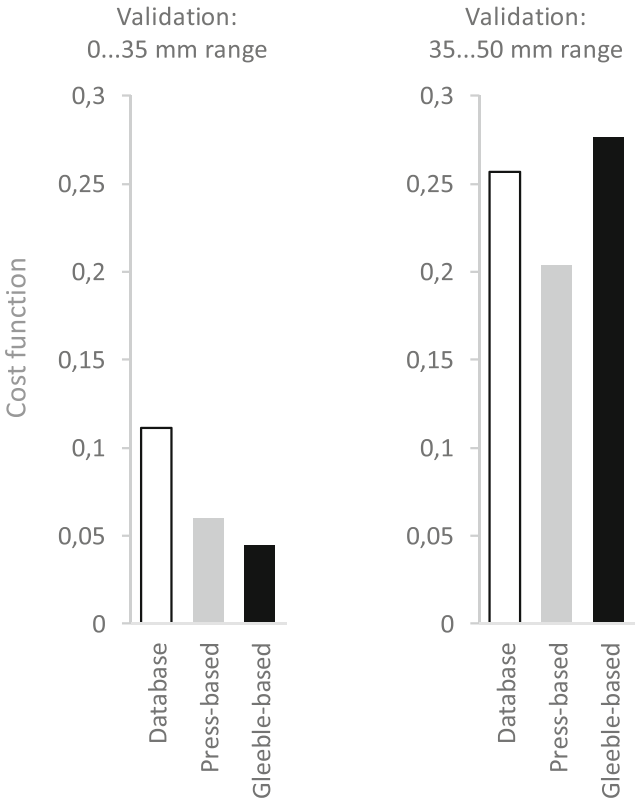

Fig. 16 Difference in cost function between the predictions of the three sets of parameters, with respect to the semi-industrial part forging experiments, for (a) displacement values smaller than 35 mm and (b) larger than 35 mm

Alternatively, the same parameter sets can be used to simulate the on-press compression experiments and confront the results to the corresponding experimental curves. Each comparison would favour one of the parameter sets but can serve to illustrate the gap between the two identification procedures.

Figure 12 illustrates the differences between the predictions of these three sets of parameters. Unsurprisingly, the predictions of the Gleeble-based parameters lay closer to the Gleeble experiments. The press-based parameter predictions are closer to the experiments than those from the database at 950 °C, while the opposite trend is observed at 1200 °C. Overall, the database and the press-based sets of parameters are close to each other. This indicates that the identification on industrial presses is a valid alternative if there is no database or specialized device available. It seems that the press-based experiments did not allow for a complete description of the stress stagnation at large strains, although almost asymptotic predictions are obtained.

In order to enhance the validation, and in view of the industrial application of the identified parameters, an additional validation was performed as the forging process of a semi-industrial component. The semi-industrial validation part shown in Fig. 13 was forged on the Loire hydraulic press, for three heating temperatures and using material from the same batch. The force/displacement curves associated with the forging operation were recorded. Each experiment was performed three times to ensure repeatability. Simulations of the forging process were performed using the Forge® software. The three sets of parameters of the Hensel–Spittel law were used for the simulations (Tables 2, 5 and 6). The force/displacement curves from each simulation are compared to the experimental ones in Fig. 14.

The value of the objective function provides a quantitative means to compare the three parameter sets. Figure 15 summarizes the objective function values calculated for each parameter set, with respect to the three reference experiments available. As expected, in the first two cases the best performance was obtained by the parameter set that was optimized on that particular dataset, respectively. The worse predictions are those of the database parameter set in both cases. However, the three cost functions are very different from each other with respect to the Gleeble experiments, while they are much closer to each other when compared to the on-press experiments. It seems that the press-based experiments are less discriminant than the plastometer ones.

The semi-industrial forging validation experiments were best predicted by the press-based parameter set, while the Gleeble-based parameters led to a result that was slightly worse than the database. A finer analysis can be made by analysing the beginning of the force-displacement curves over the first 35 mm of the stroke, where the forging force is mainly governed by the material response. The results, visible in Fig. 16a, tend to confirm that the Gleeble-based parameters best describe the material response, followed relatively closely by the press-based parameters. For the remainder of the stroke (Fig. 16b), the accuracy of the press-based parameters becomes the best, probably in connection with the influence of the friction and heat-transfer parameters, which are notoriously important in forging simulations, especially when the contact surface becomes significant. Again, the database parameters are improved by both identification approaches.

Conclusion

In this paper, a pragmatic method was proposed for the parameter identification of constitutive laws with applications to hot forging. Industrial presses were used to produce the reference experiments for identification. The prerequisite for applying the proposed methodology included the instrumentation of the press with displacement sensors and a force cell, the identification of heat transfer and friction coefficients, and an inverse method involving the FE simulation of the compression experiments.

The proposed identification procedure was applied to a 42CrMo4 steel. The resulting parameters showed a better accuracy when compared to those from a standard material

database. The accuracy level was inferior to that provided by specialized plastometers; the differences in predicted stress-strain curves was less than 40 MPa in all cases. For a semi-industrial validation problem, the proposed methodology led to accurate results, emphasizing the equal importance of the material, friction and heat transfer parameters in forging simulations. In conclusion, the proposed methodology offers a pragmatic alternative for parameter identification of hot forging constitutive laws in an industrial context, especially when the same forging equipment is used for the identification and the future forging applications.

Acknowledgments The authors are grateful to Dr. Valeriy Pidvysotskyy and Prof. Roman Kuziak from IMŻ Gliwice (Poland) who performed the Gleeble experiments. The press-shop experimental work was carried out with substantial contributions from Alexandre Fendler, Sébastien Burgun and Stéphane Mathieu (from Arts et Metiers) and Josselin Schumacker (from AMValor). The DIL805 plasto-dilatometer experiments were performed at ABS Centre Métallurgique (ACM), Metz (France).

Funding The first author received funding from the French Ministry of National Education, Higher Education and Research.

Compliance with ethical standards

Declaration of interest None.

References

1. Avrami M (1939) Kinetics of Phase Change. I General Theory. *J. Chem. Phys.* 7(12):1103–1112. https://doi.org/10.1063/1.1750380
2. Sandström R, Lagneborg R (1975) A model for hot working occurring by recrystallization. *Acta Metall.* 23(3):387–398. https://doi.org/10.1016/0001-6160(75)90132-7
3. McQueen HJ (1982) Review of Simulations of Multistage Hot-Forming of Steels. *Can. Metall. Q.* 21(4):445–460. https://doi.org/10.1179/cmq.1982.21.4.445
4. Sellars CM, Tegart WJMG (1972) Hot Workability. *Int. Metall. Rev.* 17(1):1–24. https://doi.org/10.1179/imtlr.1972.17.1.1
5. Luton MJ, Sellars CM (1969) Dynamic recrystallization in nickel and nickel-iron alloys during high temperature deformation. *Acta Metall.* 17(8):1033–1043. https://doi.org/10.1016/0001-6160(69)90049-2
6. Pauskar P, Shivpuri R (1999) Microstructure and Mechanics Interaction in the Modeling of Hot Rolling of Rods. *CIRP Ann.* 48(1):191–194. https://doi.org/10.1016/S0007-8506(07)63163-1
7. Hensel A, Spittel T (1978) Kraft und Arbeitsbedarf bildsamer Formgebungsverfahren. Leizig, VEB Deutscher Verlag für Grundstoffindustrie
8. Jäckel I (1991) Application-oriented modelling of hot yield strength of metallic materials. *Steel Res.* 62(10):441–446. https://doi.org/10.1002/srin.199100425
9. Gavrus A, Massoni E, Chenot JL (1998) The analysis of inelastic behaviour formulated as an inverse rheological approach. *Meas. Sci. Technol.* 9(6):848–863. https://doi.org/10.1088/0957-0233/9/6/002
10. Bariani PF, Dal Negro T, Bruschi S (2004) Testing and modelling of material response to deformation in bulk metal forming. *CIRP Ann.-Manuf. Technol.* 53(2):573–595
11. Lin YC, Chen X-M (2011) A critical review of experimental results and constitutive descriptions for metals and alloys in hot working. *Mater. Des.* 32(4):1733–1759. https://doi.org/10.1016/j.matdes.2010.11.048
12. Gelin JC, Ghouati O (1994) An inverse method for determining viscoplastic properties of aluminium alloys. *J. Mater. Process. Technol.* 45(1–4):435–440. https://doi.org/10.1016/0924-0136(94)90378-6
13. Gavrus A, Massoni E, Chenot JL (1996) An inverse analysis using a finite element model for identification of rheological parameters. *J. Mater. Process. Technol.* 60(1–4):447–454. https://doi.org/10.1016/0924-0136(96)02369-2
14. Kowalski B, Sellars CM, Pietrzyk M (2006) Identification of rheological parameters on the basis of plane strain compression tests on specimens of various initial dimensions. *Comput. Mater. Sci.* 35(2):92–97. https://doi.org/10.1016/j.commatsci.2005.02.024
15. Khoddam S, Hodgson PD, Jafari Bahramabadi M (2011) An inverse thermal–mechanical analysis of the hot torsion test for calibrating the constitutive parameters. *Mater. Des.* 32(4):1903–1909. https://doi.org/10.1016/j.matdes.2010.12.010
16. Mahnken R, Stein E (1994) The identification of parameters for visco-plastic models via finite-element methods and gradient methods. *Model. Simul. Mater. Sci. Eng.* 2(3A):597–616. https://doi.org/10.1088/0965-0393/2/3A/013
17. Andrade-Campos A, Thuillier S, Pilvin P, Teixeira-Dias F (2007) On the determination of material parameters for internal variable thermoelastic–viscoplastic constitutive models. *Int. J. Plast.* 23(8):1349–1379. https://doi.org/10.1016/j.ijplas.2006.09.002
18. de-Carvalho R, Valente RAF, Andrade-Campos A (2011) Optimization strategies for non-linear material parameters identification in metal forming problems. *Comput. Struct.* 89(1–2):246–255. https://doi.org/10.1016/j.compstruc.2010.10.002
19. Marie S, Ducloux R, Lasne P, Barlier J, Fourment L (2014) Inverse Analysis of Forming Processes based on FORGE environment, in Key Engineering Materials, 611, 1494–1502, Accessed: Apr. 25, 2017. [Online]. Available: http://www.scientific.net/KEM.611-612.1494
20. Pöhlandt K (1989) Materials Testing for the Metal Forming Industry. Berlin, Heidelberg: Springer Berlin Heidelberg
21. Gavrus A, Francillette H, Pham DT (2012) An optimal forward extrusion device proposed for numerical and experimental analysis of materials tribological properties corresponding to bulk forming processes. *Tribol. Int.* 47:105–121. https://doi.org/10.1016/j.triboint.2011.10.013
22. Diot S, Guines D, Gavrus A, Ragneau E (2009) Minimization of Friction Influence on the Evaluation of Rheological Parameters From Compression Test: Application to a Forging Steel Behavior Identification. *J. Eng. Mater. Technol.* 131(1):011001. https://doi.org/10.1115/1.3026543
23. Hor A, Morel F, Lebrun J-L, Germain G (2013) Modelling, identification and application of phenomenological constitutive laws over a large strain rate and temperature range. *Mech. Mater.* 64:91–110. https://doi.org/10.1016/j.mechmat.2013.05.002
24. Pietrzyk M, Jedrzejewski J (2001) Identification of parameters in the history dependent constitutive model for steels. *CIRP Ann.-Manuf. Technol.* 50(1):161–164
25. Szeliga D, Gawad J, Pietrzyk M (2006) Inverse analysis for identification of rheological and friction models in metal forming. *Comput. Methods Appl. Mech. Eng.* 195(48–49):6778–6798. https://doi.org/10.1016/j.cma.2005.03.015
26. Sztangret ł, Szeliga D, Kusiak J, Pietrzyk M (2012) Application of inverse analysis with metamodelling for identification of metal flow stress. *Can. Metall. Q.* 51(4):440–446. https://doi.org/10.1179/1879139512Y.0000000035
27. Hor A, Morel F, Lebrun J-L, Germain G (2013) An experimental investigation of the behaviour of steels over large temperature and

strain rate ranges. *Int. J. Mech. Sci.* 67:108–122. https://doi.org/10.1016/j.ijmecsci.2013.01.003

28. Zhang C, Bellet M, Bobadilla M, Shen H, Liu B (2010) A Coupled Electrical–Thermal–Mechanical Modeling of Gleeble Tensile Tests for Ultra-High-Strength (UHS) Steel at a High Temperature. *Metall. Mater. Trans. A* 41(9):2304–2317. https://doi.org/10.1007/s11661-010-0310-7
29. Pidvysotskyy V, Łapczyński Z (2018) Characterization of a steel grade on Gleeble simulator, Instytut metalurgii Zelaza, Poland, technical report B0–1613
30. Durand C, Bigot R, Baudouin C (2018) Contribution to characterization of metal forming machines: application to screw presses. *Procedia Manuf.* 15:1024–1032. https://doi.org/10.1016/j.promfg.2018.07.391
31. Diot S, Guines D, Gavrus A, Ragneau E (2007) Two-step procedure for identification of metal behavior from dynamic compression tests. *Int. J. Impact Eng.* 34(7):1163–1184. https://doi.org/10.1016/j.ijimpeng.2006.07.003
32. Wang J, Langlois L, Rafiq M, Bigot R, Lu H (2014) Study of the hot forging of weld cladded work pieces using upsetting tests. *J. Mater. Process. Technol.* 214(2):365–379. https://doi.org/10.1016/j.jmatprotec.2013.09.009
33. Venet G, Balan T, Baudouin C, Bigot R (2018) Direct usage of the wire drawing process for large strain parameter identification. *Int. J. Mater. Form.* https://doi.org/10.1007/s12289-018-01458-z
34. Emmerich M, Giotis A, Özdemir M, Bäck T, Giannakoglou K (2002) Metamodel—Assisted Evolution Strategies. In: Guervós JJM, Adamidis P, Beyer H-G, Schwefel H-P, Fernández-Villacañas J-L (eds) *Parallel Problem Solving from Nature — PPSN VII*, vol. 2439. Springer Berlin Heidelberg, Berlin, Heidelberg, pp 361–370
35. Male AT, Cockcroft MG (1964) A Method for the Determination of the Coefficient of Friction of Metals under Conditions of Bulk Plastic Deformation. *J Inst Met.* 93:38–46
36. Charpentier PL, Stone BC, Ernst SC, Thomas JF (1986) Characterization and modeling of the high temperature flow behavior of aluminum alloy 2024. *Metall. Trans. A* 17(12):2227–2237. https://doi.org/10.1007/BF02645920
37. Lee CH, Altan T (1972) Influence of Flow Stress and Friction Upon Metal Flow in Upset Forging of Rings and Cylinders. *J. Eng. Ind.* 94(3):775. https://doi.org/10.1115/1.3428250
38. Saha PK, Wilson WRD (1994) Influence of plastic strain on friction in sheet metal forming. *Wear* 172(2):167–173. https://doi.org/10.1016/0043-1648(94)90284-4